Mon. Not. R. Astron. Soc. **000**, 000–000 (0000) Printed 29 March 2007 (MN LATEX style file v2.2)

Diffusive low optical depth particle disks truncated by planets

Alice C. Quillen
Department of Physics and Astronomy, University of Rochester, Rochester, NY 14627; aquillen@pas.rochester.edu

29 March 2007

ABSTRACT
Two dimensional particle disks in proximity to a planet are numerically integrated to determine when a planet in a circular orbit can truncate a particle disk. Collisions are treated by giving each particle a series of velocity perturbations during the integration. We estimate the mass of a planet required to truncate a particle disk as a function of collision rate, related to the disk optical depth, and velocity perturbation size, related to the disk velocity dispersion. We find that for particle disks in the regime estimated for debris disks, a Neptune mass planet is sufficiently massive to truncate the disk. If both the velocity dispersion and the disk optical depth are low (dispersion less than approximately 0.02 in units of circular motion, and optical depth less than 10^{-4}) then an Earth mass planet suffices. We find that the disk is smooth and axisymmetric unless the velocity perturbation is small and the planet mass is of order or greater than a Neptune mass in which case azimuthal structure is seen near prominent mean motion resonances.

1 INTRODUCTION

Recent observations made with the Spitzer Space Telescope have added to the total number of known debris and circumstellar disks (Rieke et al. 2005; Beichman et al. 2005; Gorlova et al. 2006; Chen et al. 2006; Bryden et al. 2006; Beichman et al. 2006). Theses disks have total infrared optical depth, as estimated from the fraction of stellar light re-emitted in the infrared, in the range $\tau_{IR} \sim 10^{-3} - 10^{-5}$. Infrared spectra of many debris are well fit with a single black body temperature suggesting that they possess inner holes (Chen et al. 2006). If the disk extended to smaller radii then the spectra would be better fit with a multi-temperature model. Planets are suspected to be responsible for the inner clearings (e.g., Kalas et al. 2005; Moro-Martin & Malhotra 2005; Quillen 2006; Chen et al. 2006).

The fraction of starlight absorbed by the dust is related to the timescale between dust particle collisions. Here we focus on collisions as they are expected to make significant modifications to the dynamics. The relation between the fraction of starlight absorbed by the dust and the collision timescale depends on the width and radius of the disk. A ring at radius r with width dr and optical depth normal to the disk plane, τ_n, has total surface area $A = 2\pi r dr \tau_n$ however at radius r the starlight passes through a sphere of area $4\pi r^2$. For low optical depth systems the infrared optical depth is related to the disk optical depth by

$$\tau_n \approx \frac{2r}{dr}\tau_{IR}. \quad (1)$$

We expect that the disk optical depth, τ_n, exceeds τ_{IR} by a modest factor ($dr < r$) and that τ_n is the same order of magnitude as τ_{IR} unless the ring is very narrow. The infrared optical depth measurements allow us to crudely estimate the normal disk optical depth and so collision timescale in the disk, though when possible, direct imaging in the infrared can provide better measurements (e.g., Marsh et al. 2005).

Planets have been proposed to explain the morphology of a number of systems with dusty disks (e.g., Ozernoy et al. 2000; Wilner et al. 2002; Quillen & Thorndike 2002; Wyatt 2003; Deller & Maddison 2005), however most models do not take into account collisions between particles in the disk. The collision timescale, t_{col}, for the dust particles can be estimated from the optical depth, τ_n, normal to the disk plane,

$$t_{col} \sim (3\tau_n n)^{-1} \quad (2)$$

(Hanninen & Salo 1992) where n is the mean motion at radius r. As emphasized by Dominik & Decin (2003) and Wyatt (2005), for most debris disks the collision timescale between particles is shorter than the Poynting-Robertson drag timescale and so collisions should be considered when interpreting the evolution and morphology of these disks. Quillen (2006) proposed that the steep inner edge of Fomalhaut's disk might be due to the removal (by the planet) of particles scattered interior to the disk edge by collisions. Quillen (2006) suggested that the chaotic zone near the corotation region is a likely location for disk truncation. Disk structure has not yet been studied using numerical simulations that incorporate both perturbations by a planet and collisions on a timescale consistent with that expected for debris disks. That is what we aim to do here.

For disk optical depths in the regime of debris disks, $\tau_n \lesssim 10^{-2}$, spiral density waves cannot be driven at Lindblad resonances (Quillen 2006; this regime is also discussed in the context of planetary rings by Franklin et al. 1980; Hanninen & Salo 1992; Lissauer & Espresate 1998; Espre-

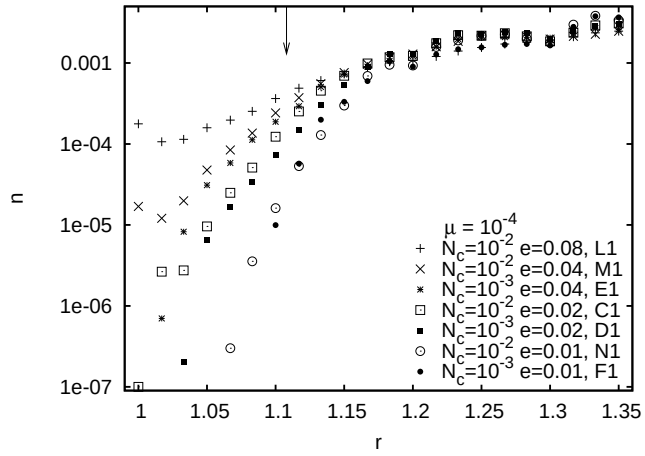

Figure 1a. Azimuthally averaged density as a function of radius for simulations L1,M1,E1,C1,D1,N1 and F1 listed in table 1. These simulations have different numbers of collisions per orbit and velocity perturbations, but the same planet mass ratio, $\mu = 10^{-4}$. Radii are given in units of the planet's semi-major axis. Arrows are drawn at the radii corresponding to the location of the chaos zone boundary at $r = 1 + 1.5\mu^{2/7}$ for each planet mass ratio.

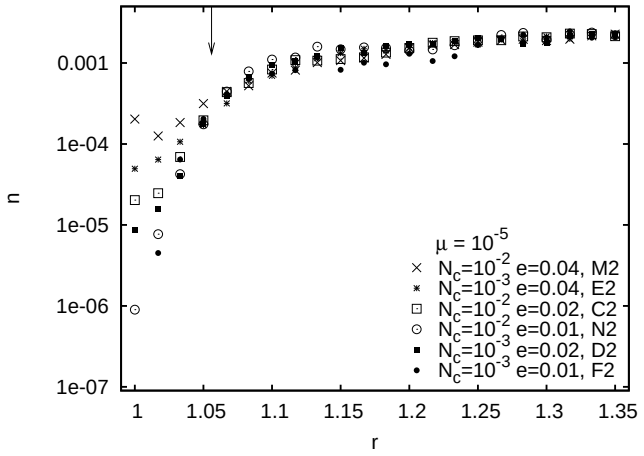

Figure 1b. Similar to 1a except simulations M2,E2,C2,N2,D2, and F2 are shown with a planet mass ratio of $\mu = 10^{-5}$.

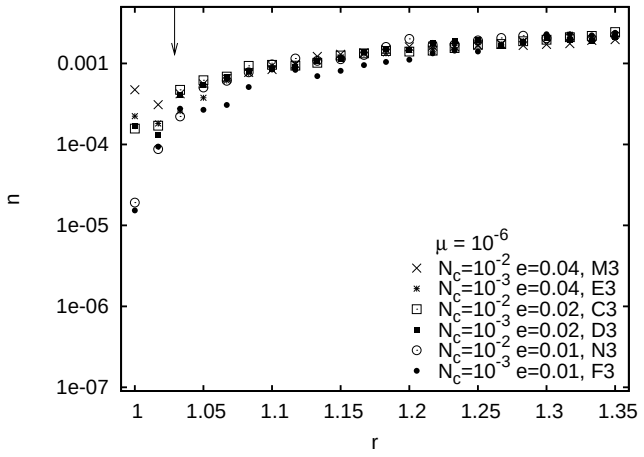

Figure 1c. Similar to 1a except simulations M3,E3,C3,D3,N3, and F3 are shown with a planet mass ratio of $\mu = 10^{-6}$.

sate & Lissauer 2001). However collision induced angular momentum transfer causes a thin disk to diffuse radially and become wider. A particle ring has two characteristic timescales (Brahic 1977), the collision timescale, t_{col}, that is related to the disk optical depth, and the diffusion timescale, t_{diff}, that depends on both the disk velocity dispersion and collision timescale.

The radial evolution of an isolated particle ring can be described with a diffusion equation

$$\frac{\partial N}{\partial t} = \frac{\partial}{\partial r}\left(D\frac{\partial N}{\partial r}\right) \tag{3}$$

where $N(r)$ is the number density as a function of radius r, (e.g., Petit & Henon 1987 equation 48 and Lithwick & Chiang 2007 equation 11). The diffusion coefficient, D, depends on the collision timescale and velocity dispersion, u^2, in the disk,

$$D \sim \frac{u^2}{t_{col} n^2}. \tag{4}$$

This diffusion coefficient is similar to a viscosity and can be estimated by considering the mean free path and particle velocity differences set by the epicyclic amplitude (e.g., Murray & Dermott 1999). As the collision time depends on the number density, the diffusion coefficient can depend on N (Petit & Henon 1987; Lithwick & Chiang 2007).

In this paper we adopt a diffusive approach toward simulating the affect of collisions on a particle disk in proximity to a planet. When the disk optical depth is low, many orbits pass between collisions. During this time particles can be integrated directly under the influence of only gravity. Previous works simulating collisions adopt a statistical method for predicting when each particle suffers a collision and its affect (e.g., Espresate & Lissauer 2001; Melita & Woolfson 1998), or search for close approaches between particles and then compute momentum changes for both particles (e.g. Lewis & Stewart 2000; Charnoz et al. 2001; Lithwick & Chiang 2007). In this work we adopt the first approach. We only perturb particles on a mean collision timescale and compute a perturbation to the particle's momentum. Both the collision timescale and momentum perturbation are chosen independent of the particle distribution (similar to the approach by Espresate & Lissauer 2001). A more sophisticated simulation would allow the particle distribution to set both quantities (e.g., Melita & Woolfson 1998). However this requires additional computational effort, either by computing close approaches carefully (Charnoz et al. 2001), letting the computed collisions depend on a numerical grid (Lithwick & Chiang 2007) or integrating sufficient numbers of particles that the velocity distribution is well sampled (Melita & Woolfson 1998).

2 NUMERICAL INTEGRATIONS

Numerical integrations were carried out in the plane, using massless particles under the gravitational influence of only the star and a massive planet with zero eccentricity, $e_p = 0$,

and semi-major axis, $a_p = 1$, using a conventional Burlisch-Stoer numerical scheme. We have not included the effect of radiation forces on the particles. Initial particle mean anomalies and longitudes of perihelia were randomly chosen. In each simulation 1000 particles were integrated for $\sim 10^5$ planetary orbital periods.

Each particle suffers collisions with a mean collision rate set by the collision timescale. The parameter we use to describe the collision rate is the number of collisions per planet orbit for an individual particle given by $N_c \approx P/t_{col}$, where P is an planet orbital period. The parameter N_c is related to the normal disk optical depth by $N_c \approx 18\tau_n$ (Hanninen & Salo 1992). Each planetary orbit, the number of collisions is computed from the total number of particles in the simulation and the collision rate. The particles that receive collisions are chosen randomly from those integrated. These particles receive perturbations to their momentum at a randomly chosen time during the orbit.

If a particle suffers a collision its radial velocity is adjusted to damp the energy,

$$v_r \rightarrow \epsilon v_r \tag{5}$$

where $-1 < \epsilon \leqslant 1$. Here we have set $\epsilon = 0$. As the particle angular momentum per unit mass is given by rv_ϕ, the above velocity perturbation only affects the particle's energy and not its angular momentum. Had we not restricted our simulations to zero eccentricity planets we would have required the radial velocity perturbation to depend on the mean set by the distribution of particles. The tangential velocity is given a random kick

$$v_\phi \rightarrow v_\phi + \Delta v \tag{6}$$

where Δv is chosen from a normal distribution with dispersion σ_{dv}. The change to the tangential velocity changes the particle's angular momentum.

Because the velocity perturbation at each collision, Δv, is chosen from a normal distribution its expectation is zero. While total angular momentum should not drift rapidly, angular momentum is not conserved during the simulation. Adjustment or redistribution of angular momentum following collisions would be required to conserve angular momentum (e.g., as explicitly described by Melita & Woolfson 1998). We do not chose to do this as we continually regenerate particles that have scattered outside the region of interest. To conserve angular momentum computational time would have been wasted integrating particles that diffuse away from the planet as well as toward it. Our adopted procedure allows us to simulate a diffusive disk with minimal time spent integrating particles outside the region near the planet.

Particle initial semi-major axes were chosen to lie between 1.4 and 1.5 times the semi-major axis of the planet. This way the particles were allowed to diffuse from larger radius, approaching the planet. Particles are removed from the simulation if they have a semi-major axis greater than 1.6 or less than 0.7, have an eccentricity greater than 0.5 or are unbound and if they move closer to the planet than 1/10 of its Hill radius. Particles that are removed from the simulation are regenerated choosing their orbital parameters in the same way as the initial particles were chosen. This ensures that a constant number of particles is integrated at all times.

The initial particle eccentricities were drawn from a Rayleigh distribution with a mean eccentricity of e_{init} that is chosen to match the velocity perturbation parameter, σ_{dv} or

$$e_{init} = \frac{\sqrt{8}\sigma_{dv}}{v_K}. \tag{7}$$

where v_K is the velocity of a particle undergoing circular motion at the radius of the planet. A particle in a nearly circular orbit with eccentricity e has radial velocity component $\frac{v_r}{v_K} = e \sin nt$ and tangential component $\frac{v_\phi}{v_K} = (1 + \frac{e}{2}\cos nt)$. A distribution of particles with the same eccentricity and random mean longitudes and longitudes of periastron has radial dispersion $\frac{<v_r^2>}{v_K^2} = \frac{e^2}{2}$ and $\frac{<(v_\phi - 1)^2>}{v_K^2} = \frac{<v_r^2>}{4v_K^2} = \frac{e^2}{8}$. This last expression accounts for the factor of $\sqrt{8}$ in equation 7. We describe and refer to simulations in terms of either the velocity perturbation, σ_{dv}, or the mean initial particle eccentricity, e_{init}, as they are directly related to one another.

A steady state is reached after the disk has had time to diffuse from the generation region (at a radius of 1.4-1.5) to the particle removal region, near the planet's orbital radius. We checked that the radial velocity dispersion distant from the planet (greater than $r \sim 1.2$) is that expected from perturbations given to the tangential velocity perturbation at each collision or $< v_r^2 > \approx 4\sigma_{dv}^2$. This is consistent with a distribution of particles with a mean eccentricity of $< e > = e_{init} = \frac{\sqrt{8}\sigma_{dv}}{v_K}$. Because the radial velocity component is damped at each collision the mean particle eccentricity does not significantly increase past this value except near the planet.

A density distribution is created from particle positions when the planet has the same location in each planetary orbit. To ensure that the density distribution is smooth and has a high dynamic range, we have added the 1000 particle positions from 1000 different timesteps. We work in units of the planet's semi-major axis, a_p, and orbital period. The mass of the planet is described in terms of its mass ratio, μ, the ratio of the planet mass to that of the central star. We describe the velocity perturbation σ_{dv} in units of the velocity of a particle in a circular orbit, v_K, or in terms of the associated initial particle eccentricity, e_{init}.

3 SIMULATIONS

The simulations we discuss have parameters listed in Table 1. We relate the simulation parameters to quantities that can be constrained by observations, the disk normal optical depth, τ_n, and the velocity dispersion that is related to the disk thickness. We have run simulations for three different planet mass ratios, $\mu = 10^{-4}, 10^{-5}$ and 10^{-6}, two different collision rates, $N_c = 10^{-2}$ and 10^{-3} collisions per particle per orbit corresponding to disk normal optical depths $\tau_n = 0.5 \times 10^{-3}$ and 0.5×10^{-4} and four different velocity perturbation sizes. In Table 1 the velocity perturbation sizes are listed in terms of the initial mean eccentricity e_{init} where $\sigma_{dv}/v_K = e_{init}/\sqrt{8}$ and are related to the disk velocity dispersion by $(u/v_K)^2 \approx e_{init}^2/2$.

Azimuthally averaged density profiles (number density as a function of radius) after equilibrium is reached are shown in Figures 1a - 1c where each figure shows simulations with only one planet mass. A comparison of Figures

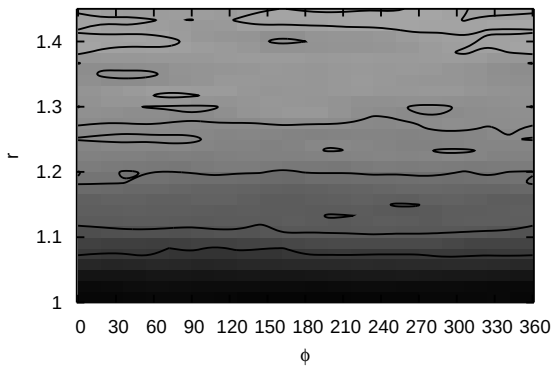

Figure 2a. Number density as a function of r and ϕ for simulation C2 with planet mass ratio $\mu = 10^{-5}$. Little structure is seen in the disk. Contours intervals are on a linear scale. The dark color shows low density regions whereas the light regions show high density regions.

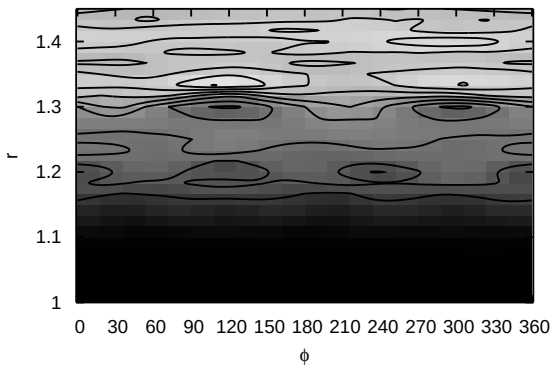

Figure 2b. Number density as a function of r and ϕ for simulation F1 with planet mass ratio $\mu = 10^{-4}$. Structure is seen in this disk associated with mean motion resonances. The 2:3 mean motion resonance is located at $r = 1.31$ and the 3:4 mean motion resonances at 1.21. Both resonances are associated with structure in the disk.

1a - 1c suggests that the radius at which the particle number density drops is related to the planet mass.

In the collisionless restricted 3 body system there is an abrupt change in dynamics in the corotation region at a semi-major axis that we refer to as the boundary of the chaotic zone. The width of this zone has been measured numerically and predicted theoretically by predicting the semi-major axis at which the first order mean motion resonances overlap (Wisdom 1980; Duncan et al. 1989; Murray & Holman 1997). In our figures we have with an arrow marked the chaotic zone boundary at a radius $r_z = a_p + da_z$ with the distance between the planet and chaotic zone $da_z = 1.5 a_p \mu^{2/7}$ (Wisdom 1980; Duncan et al. 1989) for the different simulations. We see from the figures that this boundary is approximately the location at which the radial profiles suffer a drop near the planet, as would be expected from the change in the dynamics due to overlap of mean motion resonances (Wisdom 1980; Murray & Holman 1997; Quillen & Faber 2006).

We note that the density drops before the chaotic zone boundary for the simulations with the most massive planets. The simulations with the most massive planet and the steepest profiles are also the ones that show the most structure. Figures 2a and 2b display density distributions as a function of radius and angle for simulations C2 and F1. We find for planet mass ratios equal to or below 10^{-5} little structure is evident in the density distribution. However for a planet mass ratio of 10^{-4} and low values of the velocity perturbation, structure at strong mean motion resonances such as the 3:2 and 3:4 resonance is present. When the resonances are strong, trajectories can become planet orbit crossing. Particles that diffuse into these regions are removed from the simulation (primarily because of their high eccentricity) causing structure in the surface density (as seen in figure 2b) and a reduction in the density profile at a radius larger than the chaotic zone boundary. This is likely to account for the density drop exterior to the chaotic zone boundary evident in the profiles shown in figure 1a.

In Figure 3 we show profiles for the 3 simulations with the same collision rate and perturbation but different planet masses. The radius has been been rescaled so that the chaotic zone boundaries for the $\mu = 10^{-4}$ and $\mu = 10^{-6}$ simulations align with that of the $\mu = 10^{-5}$ simulation. In other words r has been rescaled in this figure by a factor of $(10^{-5}/\mu)^{2/7}$. Here we see that this radius does give an estimate for the radius at which a disk is likely to suffer a drop in density due to removal of particles by the planet. The rescaled profiles do not lie exactly on top of each other; the lower mass planet simulations have shallower profiles in the inner part of the disk after rescaling. The disk slopes are not self similar after rescaling, implying that the disk profile shape is not solely a function of the distance to the chaotic zone.

The slope of the disk edge is dependent on the collision rate and perturbation size as well as the planet mass. In figures 4a, 4b, and 4c, we show profiles for the same number of collisions per orbit and collision velocity perturbation sizes but for different planet masses (and without rescaling the radius). The simulations shown in Figure 4b have twice the velocity perturbation size and the same collision rate as those shown in Figure 4a whereas those shown in Figure 4c have the same velocity perturbation size but a tenth the number of collisions per orbit as those shown in Figure 4a. We find that a larger change in the profile shape is caused by variation in the velocity perturbation parameter σ_{dv} than variation by the same factor in the collision rate N_c.

3.1 Diffusive descriptions for the density drop

We now discuss diffusive descriptions for the disk edge to better understand the parameters affecting the decrease in particle density near the planet. Since the velocity dispersion is $u^2 \approx < v_r^2 >$ and $< v_r^2 > \sim 4\sigma_{dv}^2$ we estimate that the diffusion coefficient (equation 4) is

$$D \approx \frac{4\sigma_{dv}^2}{t_{col} n^2}. \quad (8)$$

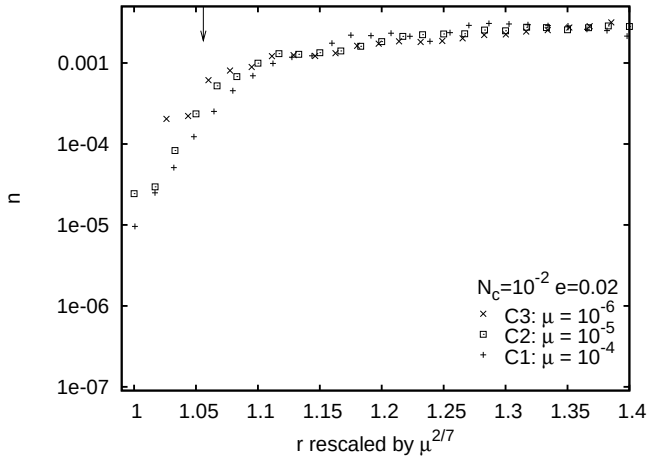

Figure 3. Azimuthally averaged density as a function of radius for simulations with different planet mass ratios C3,C2, and C1 but the same collision rate and velocity perturbation size. Here the radius has been rescaled by a factor of $(10^{-5}/\mu)^{2/7}$ so the chaotic zone boundaries for the three simulations line up.

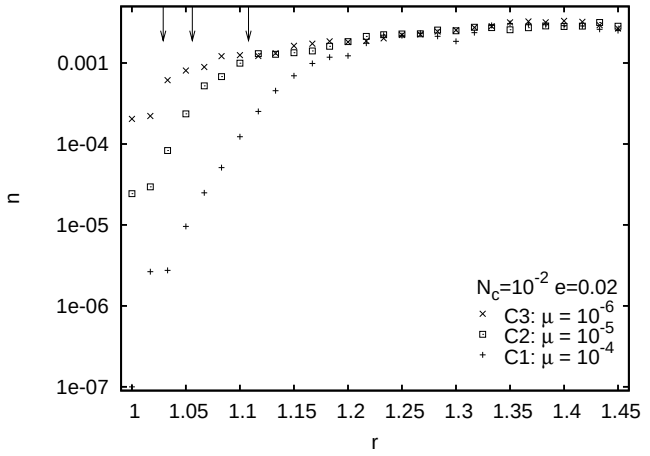

Figure 4a. Azimuthally averaged density as a function of radius for simulations with different planet mass ratios but the same collision rate and velocity perturbation sizes. Here simulations C3,C2, and C1 are shown.

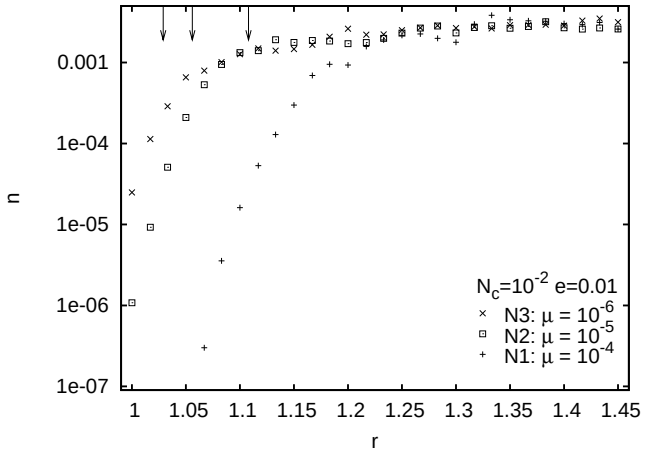

Figure 4b. Same as figure 4a but for simulations N3,N2, and N1. These simulations have twice the velocity perturbation size and the same collision rate as those shown in 4a.

In units of the square of the planet semi-major axis divided by the rotation period,

$$D \approx 4N_c \left(\frac{\sigma_{dv}}{v_K}\right)^2 = \frac{e_{init}^2 N_c}{2}. \quad (9)$$

The diffusion equation for an isolated ring, Equation 3, must be modified to include the effect of the planet. When a steady state is reached ($\frac{\partial N}{\partial t} \approx 0$), a simple model is

$$\frac{\partial}{\partial r}\left(D\frac{\partial N}{\partial r}\right) \approx \left.\frac{\partial N}{\partial t}\right|_{planet}, \quad (10)$$

(e.g., Quillen 2006) where the right hand side represents the rate that particles are removed from radius r because of perturbations from the planet. This term is expected to be a function of planet mass and distance to the planet but is also a function of the particle velocity distribution or eccentricity distribution.

We assume that there is only one important scale in the problem, the distance between the planet and the chaotic zone boundary, $da_z = 1.5\mu^{2/7}$. We rewrite equation 10 with in terms of variable $y = \frac{r-r_p}{da_z}$ and assuming that the diffusion coefficient is independent of r and N,

$$\frac{\partial^2 N}{\partial y^2} \approx \frac{da_z^2}{D}\left.\frac{\partial N}{\partial t}\right|_{planet}. \quad (11)$$

A simple form for the right hand side of equation 10, describing removal of particles by the planet, would be

$$\left.\frac{\partial N}{\partial t}\right|_{planet} \sim \begin{cases} \frac{Nf(y)}{t_{remove}} & \text{for } 0 < y < 1 \\ 0 & \text{for } y \geqslant 1 \end{cases} \quad (12)$$

When $f(y) = 1$, the solution to equation 11 is

$$N(y) \propto e^{yl} \quad (13)$$

with inverse scale length

$$l \sim \sqrt{\frac{da_z^2}{t_{remove}D}}. \quad (14)$$

If $f(y) = 1 - y$, then $N(y)$ is an Airy function and if $f(y) = \exp(-y)$ (as might be expected from lifetime measurements in collisionless integrations; David et al. 2003) the solution is a modified Bessel function. These solutions also behave in an exponential manner with an inverse scale length that is of the same order of magnitude as l. Figures 1a - 1c, 4a - 4c show that the density profiles do approach an exponential form near the planet where the density gradient is steepest. In parameters related to our simulations we expect the inverse scale length

$$l \sim 2t_{remove}^{-1/2}\mu^{2/7}N_c^{-1/2}e_{init}^{-1}. \quad (15)$$

From the simulations we measure the density near the planet compared to that away from the disk edge or specifically the log of this ratio

$$\Delta \equiv \log_{10}\left(\frac{N(y=0)}{N(y \gtrsim 1)}\right). \quad (16)$$

Equations 13 and 15 suggest that Δ depends on parameters describing our simulations, such as the planet mass ratio, collision rate and velocity perturbation size, however the

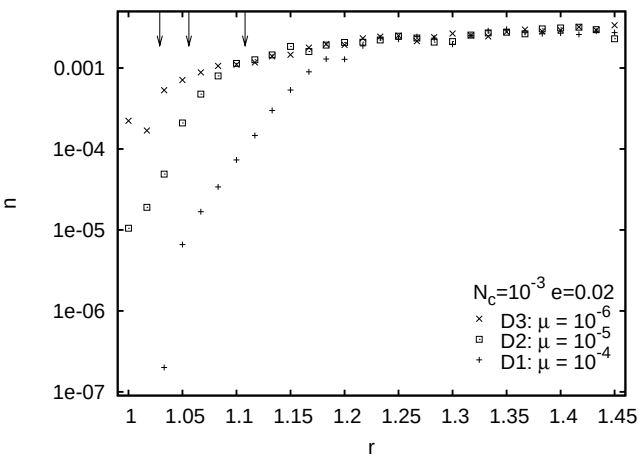

Figure 4c. Same as figure 4a but for simulations D3,D2, and D1. These simulations have the same velocity perturbation size but a tenth the number of collisions per orbit as those shown in 4a.

above approximations and assumptions may be too simplistic to give an accurate prediction for the inverse scale length l. Furthermore l contains the unknown timescale, t_{remove}.

The density decrement, Δ, measured from the radial profiles shown in Figures 1a - 1c, is plotted in Figures 5a and 5b. As predicted by equation 15, our measured density decrement is consistent with a power law function of the simulation parameters. Also as we expected Δ increases with increasing planet mass ratio, and decreases with increasing collisions rate and velocity perturbation size. To measure the exponents, we have fit lines to the density decrements finding pretty good correspondence with the following function that is also plotted in Figures 5a and 5b,

$$\log_{10}\Delta \approx 0.12 + 0.23\log_{10}\left(\frac{\mu}{10^{-6}}\right) - 0.1\log_{10}\left(\frac{N_c}{10^{-2}}\right) - 0.45\log_{10}\left(\frac{e_{init}}{0.01}\right) \quad (17)$$

This function implies that the inverse scale length

$$l \sim 3.0\left(\frac{\mu}{10^{-6}}\right)^{0.23}\left(\frac{N_c}{10^{-2}}\right)^{-0.1}\left(\frac{e_{init}}{0.01}\right)^{-0.45}. \quad (18)$$

A comparison between the measured scale length above (equation 18) and that predicted by equation 15 reveals some inconsistencies. Equation 15 implies that the length scale should be proportional to $N_c^{-1/2}e_{init}^{-1}$ rather than $N_c^{-0.1}e_{init}^{0.45}$ as we find above. The above function measured l combined with equation 15 would imply that

$$t_{remove} \sim 145\left(\frac{\mu}{10^{-6}}\right)^{0.11}\left(\frac{N_c}{10^{-2}}\right)^{-0.8}\left(\frac{e_{init}}{0.01}\right)^{-1.1} \quad (19)$$

in orbital periods. It is not clear why the removal timescale would increase with planet mass. Had we used a larger scale for the distance than the distance to the chaotic zone boundary in equations 12 and 14 then the form of t_{remove} would have changed. It is expected that t_{remove} depends on the velocity perturbation size as we do expect the particle lifetime near the planet to depend on particle eccentricity, with shorter lifetimes or removal timescales at higher particles eccentricities. Perhaps the particle lifetime depends on the collision rate because particles tend to diffuse to higher and higher eccentricity between collisions. Our measured l is not as strong a function of N_c as predicted by equation 15. A better theoretical model for both particle lifetime and diffusion is required to better match the measured exponents of equation 18.

3.2 Disk truncation

The shallowest profiles displayed in Figures 1a - 1b represent particle disks that have sufficiently high collision rates and velocity dispersions that a planet cannot efficiently truncate the disk. It is interesting to apply our measured density decrement to estimate the minimum planet mass that can truncate a disk. We set a limit of $\log_{10}\Delta = 0.12$ (corresponding to a density drop of 20) from the shallowest simulations and solve equation 17 to find the mass ratio of a planet that cannot effectively truncate at disk of a particular collision rate and velocity dispersion. To truncate a low optical depth particle disk a planet must have mass ratio greater than

$$\log_{10}\mu \gtrsim -6 + 0.43\log_{10}\left(\frac{N_c}{10^{-2}}\right) + 1.95\log_{10}\left(\frac{e_{init}}{0.01}\right) \quad (20)$$

or in quantities more directly related to observations

$$\log_{10}\mu \gtrsim -6 + 0.43\log_{10}\left(\frac{\tau_n}{5\times10^{-3}}\right) + 1.95\log_{10}\left(\frac{u/v_K}{0.007}\right). \quad (21)$$

The function (equation 21) is plotted in figure 6 for collision rates $N_c = 10^{-2}$ and 10^{-3} collisions per orbit corresponding to disk optical depths $\tau_n = 0.5\times10^{-3}$ and 0.5×10^{-4}. Instead of plotting this minimum mass ratio as a function of e_{init} we plot as a function of velocity dispersion using $e_{init}^2 \sim 2(u/v_K)^2$. On this plot we also show a limit corresponding to the eccentricity of a particle that would allow a particle to cross from the chaos zone boundary to the planet's semi-major axis, or the limit $(u/v_K) \sim 1.5\mu^{2/7}$. We refer to this limit on the plot as μ_e.

It is interesting to compare our mass limit for disk truncation to that expected for an α accretion disk. A gaps opens in a viscous accretion disk when the torque driven by spiral density waves excited by a planet exceeds viscous inflow or

$$\mu \gtrsim 40Re^{-1} \quad (22)$$

(Lin & Papaloizou 1979; Bryden et al. 1999; Ward 1997). Here the inverse of the Reynold's number $Re^{-1} = \alpha(u/v_K)^2$. We have plotted this function on Figure 6 as a thin dotted line for $\alpha = 0.001$. We have chosen to plot a gap opening line for $\alpha = 0.001$ because it can be directly compared to the mass of a planet required for particle disk truncation for $N_c = 10^{-2}$. The viscosity and the diffusion coefficient have the same physical units. A particle disk has effective viscosity set by the diffusion coefficient of equation 4 (e.g., Murray & Dermott 1999), hence if our particle disks behaved similar to an accretion disk then for $\alpha = 0.001$ the planet mass required for gap opening (shown as a thin dotted line in figure 6) would be approximately that for $N_c = 10^{-2}$ with an effective $\alpha \sim N_c/6 \sim 0.001$.

It is interesting that the disk truncation criterion scales with velocity dispersion in the same way as the accretion disk; both require that the planet mass ratio exceed a constant times the square of the velocity dispersion. However, we find that a larger planet is required to open a gap in an accretion disk with equivalent viscosity to the diffusion coefficient in a low optical depth particle disk. This is somewhat

counter-intuitive as spiral density waves excited by a planet carry angular momentum pushing material away from the planet and they cannot be driven in a low optical depth particle disk. However collisions damp orbital eccentricity and high eccentricity orbits can be more quickly scattered by a planet. A lower mass planet might be able to truncate a particle disk because the long timescale between collisions allows particle eccentricities to grow near the planet. We suspect that as circumstellar disks lose their gas and evolve into particulate debris disks, lower mass bodies become effective at opening gaps and truncating the disk.

Figure 6 illustrates that for particle disks in the regime expected for debris disks, a Neptune mass planet is sufficiently massive to truncate the disk, and if the velocity dispersion is low ($u/v_K \lesssim 0.02$) and the disk optical depth low, $\tau_n \lesssim 10^{-4}$, an Earth mass planet suffices.

4 DISCUSSION

Here we have not considered models with dust produced in resonance (e.g., Quillen & Thorndike 2002; Wyatt 2003) but only allowed particles to diffuse inward toward resonances. In resonance, certain angles with respect to the planet have longer removal timescales than others. Effectively $\frac{\partial N}{\partial t}\big|_{planet}$ depends on the orbital elements of the particle distribution and the diffusion equation should be expanded to depend not on radius but all the orbital elements. Individual resonances may play an important role in setting the velocity dispersion of disks near larger planets, causing increased diffusion near the disk edge (e.g., Quillen 2006; Quillen & Faber 2006). We expect additional complexity and structure if particles are produced trapped in resonance or if the system is not in a steady state. The simulations were run an average of 10^5 orbits which is long compared to the age of some large debris disks. Our integration times are long because we allowed particles to diffuse toward the planet from a moderately distant location and we ran each simulation for sufficiently long enough to achieve a steady state. Additional phenomena may be discovered in evolving systems.

The simulations were carried out with a collision rate and associated collision induced velocity perturbation independent of position, however particles near the planet should have suffered fewer collisions because of the steep drop in density. Particles near the disk edge should have also suffered larger velocity perturbations as the velocity dispersion increases nearing the planet. The velocity dispersion increase (spanning a factor of a few) is not as significant as the density decrease nearing the planet (spanning orders of magnitude for the largest planet simulations). A more accurate simulation probably would have a steeper disk edge due to the decrease in collision rate near the planet and would have required longer to achieve equilibrium as a consequence.

Here we have adopted a diffusive approach toward simulating particle disks and neglected the role of the particle size distribution. If collisions are destructive then diffusion caused by collisions can still take place. However each diffusive step involves a destructive collision producing smaller bodies and these in turn have a shorter collision timescale. We imagine an effective diffusion coefficient that depends not only on local particle density but on the size distribution with the larger particles effectively having longer collisions times and smaller diffusion coefficients. The different sized particles also may have different velocity dispersions. In this case we would expect that the larger bodies would have smaller diffusion coefficients as the large bodies would have lower velocity dispersions. It is tempting though premature to predict that the different size particles would exhibit different disk morphologies as a consequence of their different collisional timescales and velocity dispersions.

It is interesting to compare our simulations to imaging studies of debris disks. Our lower mass limit (equation 21, see circle in Figure 6) is simlar to the previous limit set by Quillen (2006) for Fomalhaut. As noted by Quillen & Faber (2006) the dynamics of low free eccentricity particles near an eccentric planet is similar to low eccentricity particles near a planet in a circular orbit, so we can extend equation 21 to low eccentricity planets. A particle with zero free eccentricity is apsidally aligned with the planet and has eccentricity equal to the forced eccentricity. Observations of Fomalhaut's disk have not revealed any lumps or asymmetries in the disk, other than its eccentricity (Kalas et al. 2005), consequently the planet mass must not be high ($\mu \lesssim 10^{-4}$). Otherwise Fomalhaut's disk would look like the disk displayed in Figure 2b. Consequently we also confirm, in a different way, the upper limit for the planet mass proposed by Quillen (2006). In contrast, Epsilon Eridani's disk does show clumpy structure (Poulton et al. 2006). If particles are produced outside resonance (as explored here) then we would infer that a moderate mass planet and low dispersion disk might account for the morphology. For particles born in resonance additional study is needed to predict the morphology (for a good start on this see Krivov et al. 2007).

5 SUMMARY

We have simulated the effect of collisions on a particle disk by introducing velocity perturbations into numerical integrations of particles under the influence of gravity from a star and a single planet. We have explored the regime estimated for debris disks with total infrared optical depth in the range $10^{-3} - 10^{-5}$. We find that the planet's chaotic zone boundary is an approximate location for the disk edge for systems that have normal optical depths in the range of observed debris disks. We find that density profiles do depend on the collision timescale but are more strongly dependent on the velocity perturbation size or velocity dispersion in the disk. The simulated disk morphology is axisymmetric and smooth unless the planet mass ratio $\gtrsim 10^{-5}$ and the velocity perturbation size $\lesssim 0.02$. For higher mass ratio planets and lower velocity perturbation simulations structure is seen in the vicinity of strong mean motion resonances at locations where particles are more quickly removed from the simulation due to interactions with the planet.

From the simulations we have measured a density decrement describing the log of the density ratio of that close to the planet and that past the disk edge. The density decrement depends on powers of the planet mass ratio, collision timescale and velocity perturbation size. With a diffusion approximation this decrement represents a scale length that might in future be predicted with better understanding of particle dynamics near the planet.

We have used our numerically measured density decre-

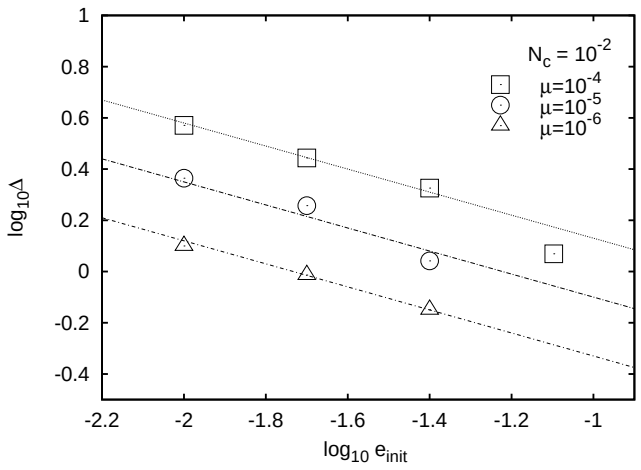

Figure 5a. The log of the density decrement, Δ, (related to the ratio of the density past the chaotic zone to that near the planet, see equation 16) versus the log of the velocity perturbation size. Only the simulations with $N_c = 10^{-2}$ collisions per orbit are plotted. Squares, circles and points represent simulations with planet mass ratio $\mu = 10^{-4}, 10^{-5}$ and 10^{-6} respectively. Also plotted is a linear function described by equation 17.

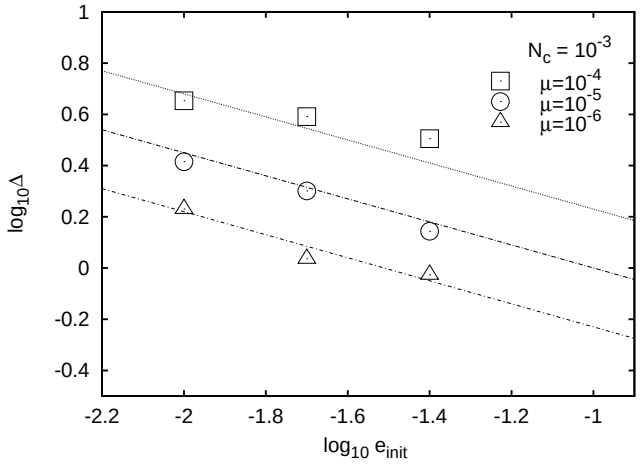

Figure 5b. Same as Figure 5a except for $N_c = 10^{-3}$.

ment to predict the mass of a planet required to truncate a particle disk (equation 21). The minimum planet mass required depends on the square of the disk velocity dispersion, similar to gap opening in an accretion disk. However we find that a lower mass planet can truncate a low optical depth disk than an accretion disk with an equivalent viscosity. The minimum planet mass also depends on the collision rate. As the collision rate is related to the disk optical depth and the velocity dispersion related to the disk thickness, equation 21 can be used to estimate the mass of an unseen planet from observations of debris disks.

I thank Sarah Maddison and Peter Faber for helpful comments. Support for this work was in part provided by National Science Foundation grant AST-0406823, and the National Aeronautics and Space Administration under Grant No. NNG04GM12G issued through the Origins of Solar Systems Program, and HST-AR-10972 to the Space Telescope Science Institute.

REFERENCES

Brahic, A. 1977, A&A 54, 895
Beichman, C. A et al. 2005, ApJ, 622, 1160
Beichman, C. A., et al 2006, ApJ, 652, 1674
Bryden, G., Beichman, C. A., et al. 2006, ApJ, 636, 1098
Bryden, G., Chen, X., Lin, D. N. C., Nelson, R. P., & Papaloizou, J. C. B. 1999, ApJ, 514, 344
Charnoz, S., Thebault, P., & Brahic, A. 2001, A&A, 373, 683
Chen, C. H. et al. 2006, ApJS, 166, 351
David, E.-M., Quintana, E.V., Fatuzzo, M., & Adams, F.C. 2003, PASP, 115, 825
Deller, A. T., & Maddison, S. T. 2005, ApJ, 625, 398
Dominik, C., & Decin, G. 2003, ApJ, 598, 626
Duncan, M., Quinn, T., & Tremaine, S. 1989, Icarus, 82, 402
Espresate, J., & Lissauer, J. J. 2001, Icarus, 152, 29
Franklin, F. A., Lecar, M., Lin, D. N. C., & Papaloizou, J. 1980, Icarus, 42, 271
Gorlova, N., Rieke, G. H., Muzerolle, J., Stauffer, J.R., Siegler, N., Young, E. T., & Stansberry, J. H. 2006, ApJ, 649, 1028
Hanninen, J., & Salo, H. 1992, Icarus, 97, 228
Kalas, P., Graham, J. R., Clampin, M. 2005, Nature, 435, 1067
Krivov, A. V., Queck, M., Lohne, T., & Sremcevic, M., 2007, A&A, 462, 199
Lithwick, Y., & Chiang, E. 2007, ApJ, 656, L524
Lin, D. N. C., & Papaloizou, J. C. B. 1979, MNRAS, 186, 799
Lewis, M. C., & Stewart, G. R. 2000, AJ, 120, 3295
Lissauer, J. J., Espresate, J. 1998, Icarus, 134, 155
Marsh, K. A., Velusamy, T., Dowell, C. D., Grogan, K., & Beichman, C. A. 2005, ApJ, 620, L47
Melita, M. D., & Woolfson, M. M. 1998, MNRAS, 299, 60
Moro-Martin, A., & Malhotra, R. 2005, ApJ, 633, 1150
Murray, C. D. & Dermott, S. F. 1999, Solar System Dynamics, Cambridge University Press, Cambridge
Murray, N., & Holman, M. 1997, AJ, 114, 1246
Poulton, C. J., Greaves, J. S., & Cameron, A. C. 2006, MNRAS, 372, 53
Ozernoy, L. M., Gorkavyi, N. N., Mather, J. C.,& Taidakova, T. A. 2000, ApJ, 537, L147
Petit, J.-M., & Henon, M. 1987, A&A, 188, 198
Quillen, A. C. 2006, MNRAS, 372, L14
Quillen, A. C., & Faber, P. 2006, MNRAS, 373, 1245
Quillen, A. C., & Thorndike, S. 2002, ApJ, 578, L149
Rieke, et al. 2005, ApJ, 620, 1010
Ward, W. R. 1997, Icarus, 126, 261
Wilner, D.J., Holman, M.J., Kuchner, M. J., & Ho, P.T.P. 2002, ApJ, 569, L115
Wisdom, J. 1980, AJ, 85, 1122
Wyatt, M. C. 2005, A&A, 433, 1007
Wyatt M. C., 2003, ApJ, 598, 1321.

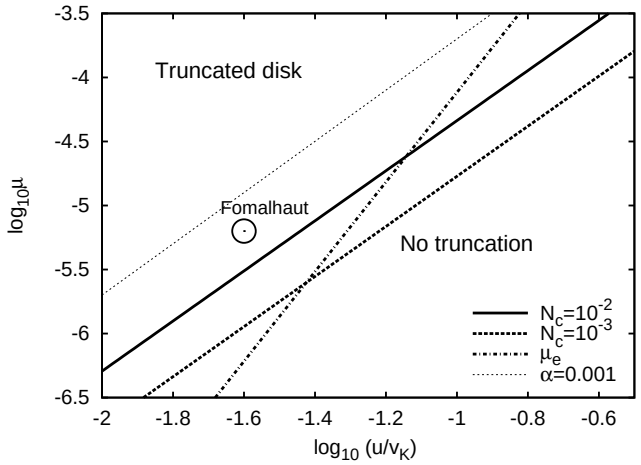

Figure 6. Disks can be truncated by planets with a mass ratio that lies above the lines drawn. The x-axis is the disk velocity dispersion. The solid and dashed line refer to particle disks with a limit set by equation 17 for $N_c = 10^{-2}$ and 10^{-3} collisions per particle per orbit, respectively. The thin dotted line is the gap opening criteria expected for an α accretion disk with $\alpha = 0.001$. The dot dashed line is a limit set by requiring that the disk thickness be lower than chaotic zone width. A circle has been placed at the estimated planet mass lower limit for a planet inside Fomalhaut's disk edge using $N_c = 3 \times 10^{-2}$ expected from the normal optical depth, $\tau_n = 1.6 \times 10^{-3}$ (Marsh et al. 2005) and velocity dispersion estimated from the disk edge slope $u/v_K \sim 0.02$ (Quillen 2006).

Table 1. List of Simulations

Name	μ	N_c	e_{init}
C1	10^{-4}	10^{-2}	0.02
C2	10^{-5}	10^{-2}	0.02
C3	10^{-6}	10^{-2}	0.02
D1	10^{-4}	10^{-3}	0.02
D2	10^{-5}	10^{-3}	0.02
D3	10^{-6}	10^{-3}	0.02
E1	10^{-4}	10^{-3}	0.04
E2	10^{-5}	10^{-3}	0.04
E3	10^{-6}	10^{-3}	0.04
F1	10^{-4}	10^{-3}	0.01
F2	10^{-5}	10^{-3}	0.01
F3	10^{-6}	10^{-3}	0.01
M1	10^{-4}	10^{-2}	0.04
M2	10^{-5}	10^{-2}	0.04
M3	10^{-6}	10^{-2}	0.04
N1	10^{-4}	10^{-2}	0.01
N2	10^{-5}	10^{-2}	0.01
N3	10^{-6}	10^{-2}	0.01
L1	10^{-4}	10^{-2}	0.08

The parameters describing the discussed simulations are as follows: The planet mass ratio is μ, and N_c is the average number of collisions suffered by each particle per planet orbit. The dispersion of the azimuthal velocity kick during each collision is given by, σ_{dv}, where $\sigma_{dv}/v_K = e_{init}/\sqrt{8}$ in units of the velocity of a particle in a circular orbit. The planet is in a circular orbit. During each collision event the radial velocity component is set to zero ($\epsilon = 0$). Particles are removed from the simulation if semi-major axis $a > 1.5$ or $a < 0.7$, eccentricity $e > 0.5$ or the particle passed within 0.1 Hill radii of the planet. Particles are generated and regenerated when removed with a semi-major between 1.4 and 1.5 and a mean eccentricity of e_{init}. Simulations were run for 10^5 planetary orbits excepting the F series that were run twice as long and the L1 simulation that was run half as long. These times are long because we allowed particles to diffuse toward the planet from a moderately distant location and we ran each simulation for sufficiently long enough to achieve a steady state.